# Constraining edifice stability and phreatic eruptions at White Island, New Zealand

Klaus Mayer[1], Bettina Scheu[1], Yan Lavallée[2], Ben Kennedy[3], Albert Gilg[4], Michael Heap[5], Patrick Baud[5], Mark Letham[3],
Cristian Montanaro[1], Laura Jacquemard[5], Noémie Pernin[5], Thierry Reuschlé[5], Donald B. Dingwell[1]

1) LMU München, Germany; 2) University of Liverpool, UK; 3) University of Canterbury, New Zealand; 4) TU München, Germany; 5) University of Strasbourg, France
Correspondence: klaus.mayer@min.uni-muenchen.de

## Introduction

White Island is New Zealand's most active volcano and is primarily characterised by phreatic and phreatomagmatic eruptions, interspersed by occasional strombolian events. It's activity became again obvious when the phreatic eruption of August 2nd, 2012, ended an eleven year lasting quiescence. The common occurrence of magma-water interaction at White Island derives from the presence of an active hydrothermal system that induces alteration of the edifice. Here, we constrain the influence of alteration

(1) on phreatic eruption conditions and
(2) on the stability of an edifice subjected to an active hydrothermal system.

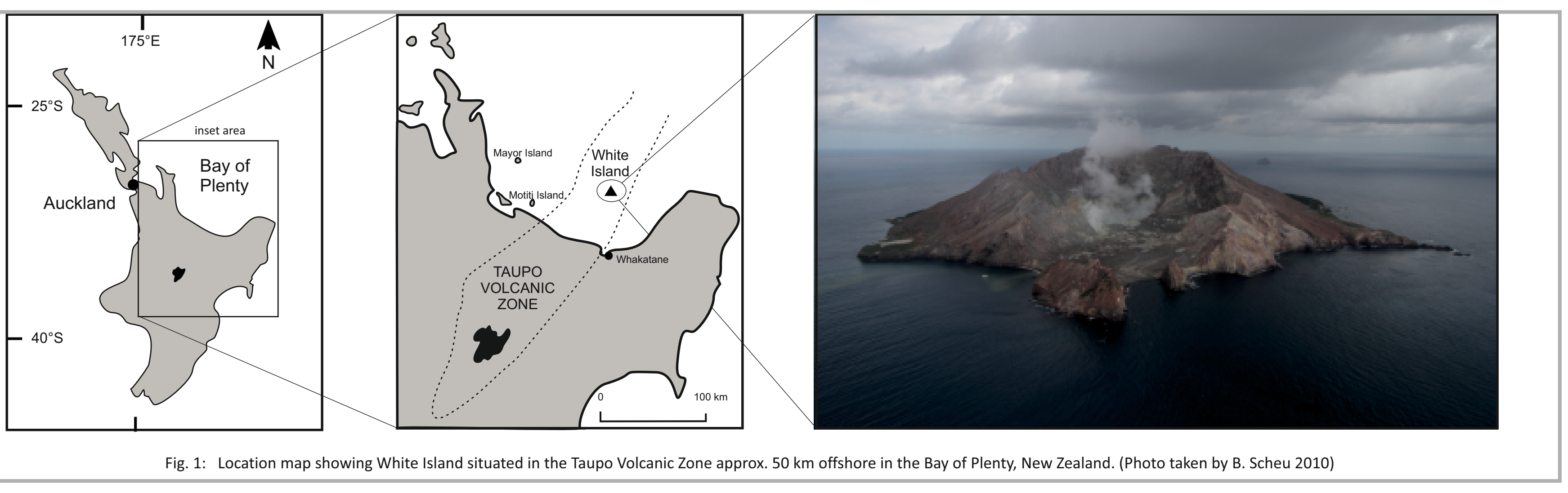

Fig. 1: Location map showing White Island situated in the Taupo Volcanic Zone approx. 50 km offshore in the Bay of Plenty, New Zealand. (Photo taken by B. Scheu 2010)

## Sample characterisation

One hydrothermally altered lava flow and four ash tuffs with different grades of alteration were sampled and investigated. In addition sulfur-rich and iron-rich crusts as well as ash/lapilli and clay from the crater floor have been collected to constrain the conditions for phreatic eruptions.

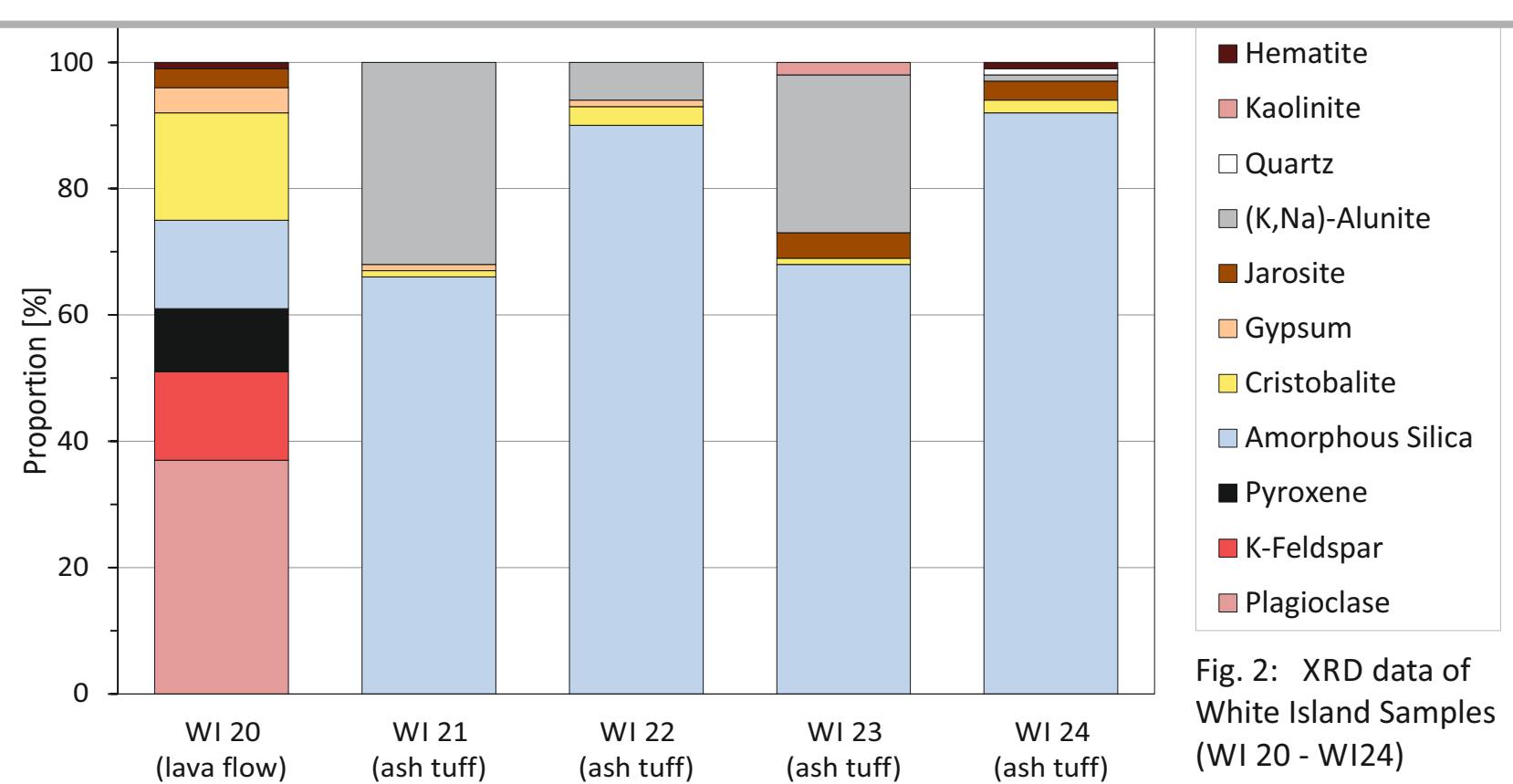

Fig. 2: XRD data of White Island Samples (WI 20 - WI24)

## Geochemical analysis

Based on XRF and XRD analysis, the mineral composition of the rhyodacytic lava flow shows the effects of hydrothermal alteration. The ash tuffs do not preserve any primary minerals or glass but are entirely altered. They contain high proportions of amorphous silica, alunite, kaolinite and other minerals, typical for hydrothermal alteration as well as high sulfur contents (Fig. 1 & 2).

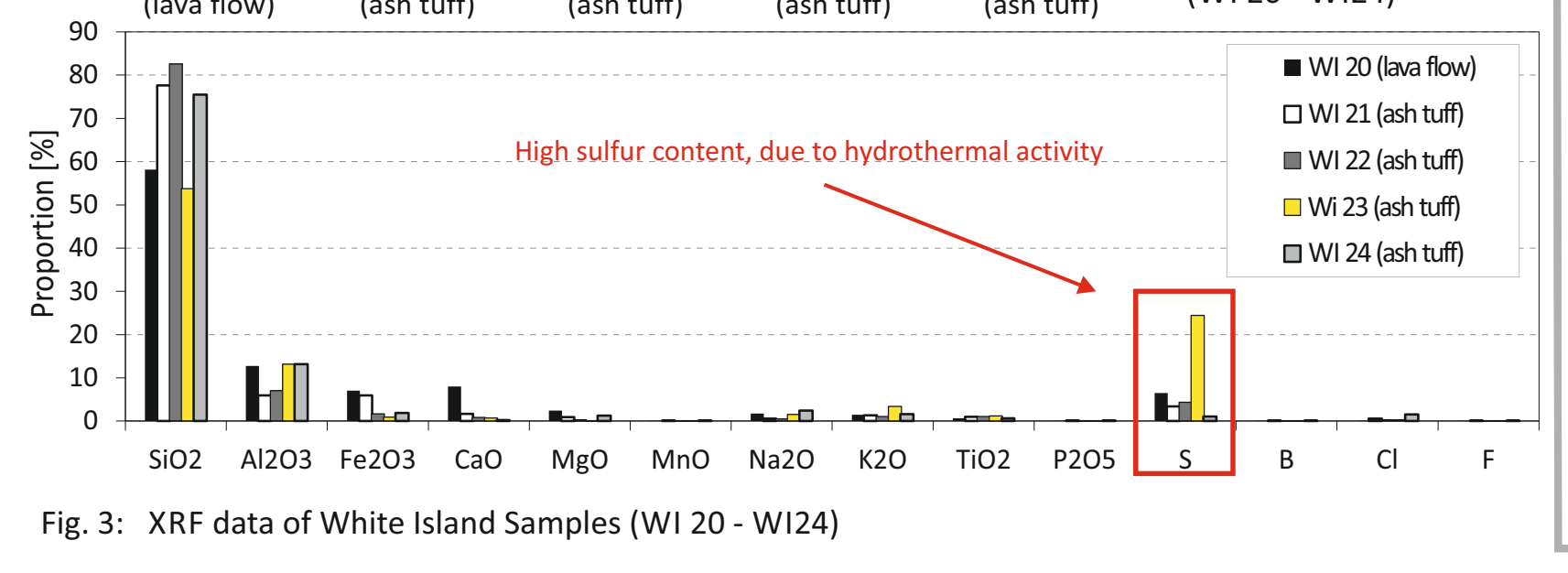

Fig. 3: XRF data of White Island Samples (WI 20 - WI24)

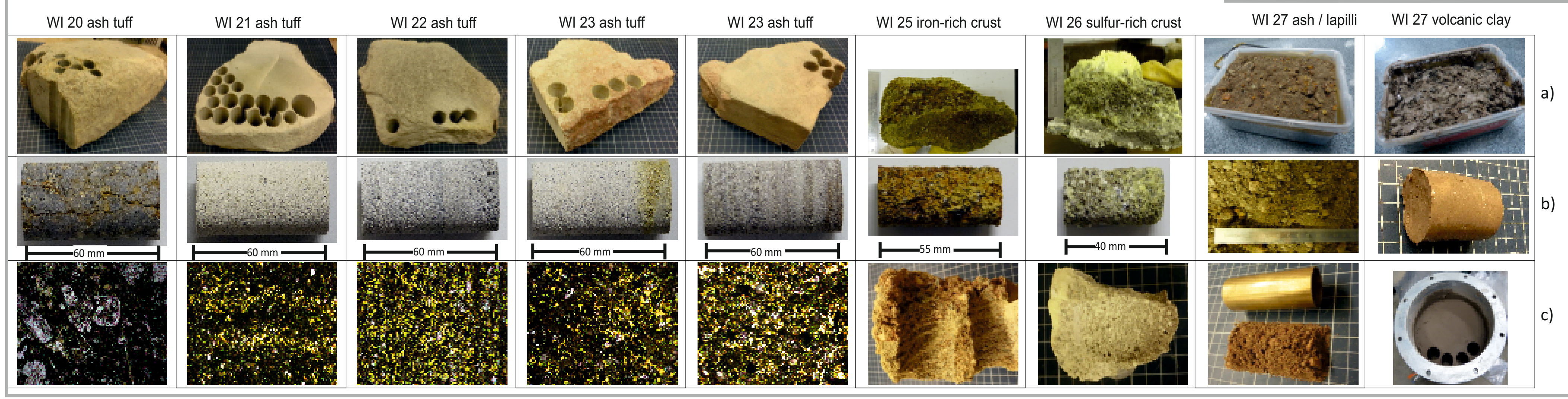

Fig. 4: Table of photos showing different stages of sample preparation and thin sections
Line a) samples before and after drilling
Line b) cores of solid samples and detail photos of ash / lapilli
Line c) thin sections photos of lava flow, ash tuffs and detail photos of iron-rich and sulfur-rich crust, ash / lapilli with sample holder and volcanic clay after consolidation. The thin section photo of the lava flow shows pyroxene phenocrysts and marginal altered plagioclase. Due to alteration, the thinsection photos of the ash tuffs show hardly any visible minerals. Note: Yellow resin (epoxy) was used to impregnate the samples.

## Rock mechanical properties

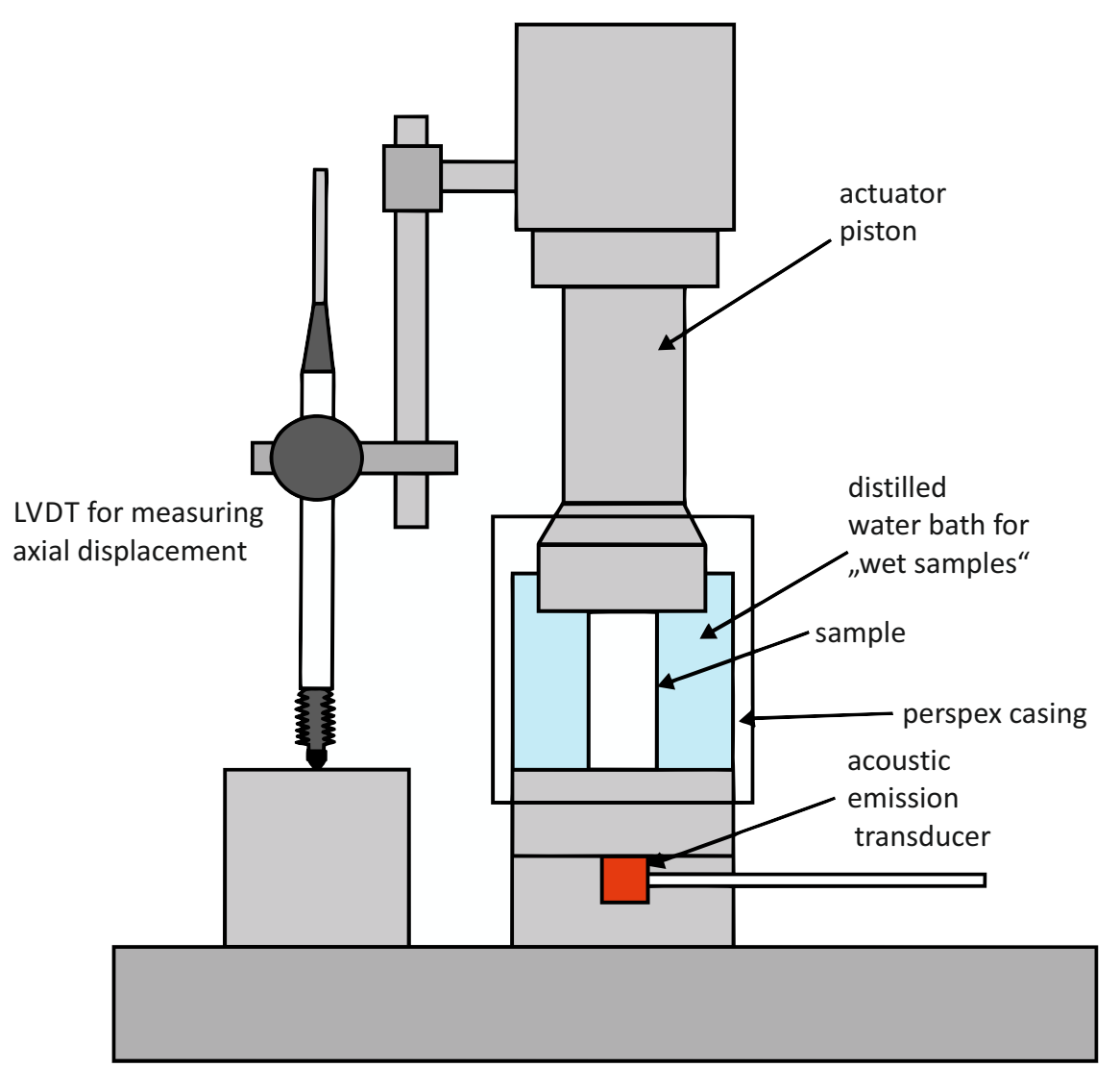

Fig. 4: Schematic sketch of a uniaxial compression apparatus from Schenkz.

Values in Table 1 have been determined at EOST (University of Strasbourg). By using an uniaxial compression apparatus (Fig. 4). Stress, axial strain, and the output of acoustic emission energy during experimentation could be measured under a variety of loading and under dry and wet environmental conditions.

The very low porous lava flow is hmoderately strong under uniaxial conditions although the presence of fractures occasionally lowers the strength as well as the ultrasonic Vp and Vs velocities. In addition it is relatively low permeable. The altered and more heterogeneous ash tuffs are weaker, more porous and permeable, compared to the lava flow. The dense and low porous iron-rich crust ranges between the ash tuffs and the lava flow concerning rock strength and ultrasonic velocities, whereas the internally very heterogeneous sulfur-rich crust is weaker and shows Vp and Vs values comparable to the ash tuffs. Ash/lapilli and the consolidated volcanic clay have the highest, respectively lowest permeabilty of all investigated samples.

Table 1: Rock mechanical properties of White Island samples, measured at the EOST (University of Strasbourg).

| | **WI 20 (lava flow)** | **WI 21 (ash tuff)** | **WI 22 (ash tuff)** | **WI 23 (ash tuff)** | **WI 24 (ash tuff)** | **WI 25 (iron crust)** | **WI 26 (sulfur crust)** | **WI 27 (ash/lapilli)** | **WI 28 (clay)** |
|---|---|---|---|---|---|---|---|---|---|
| **Density** [g/cm$^3$] | 2,66 | 2,31 | 2,18 | 2,24 | 2,19 | 2,71 | 1,97 | 2,50 | 2,68 |
| **Porosity** (open) [%] | 6,9 | 31,86 | 46,78 | 41,00 | 48,00 | 22,19 | 28,19 | 34,86 | 26,13 |
| **Permeability** [m$^2$] | $1,8\times10^{-16}$ | $2,76\times10^{-15}$ | n.m. | n.m. | n.m. | $2,84\times10^{-12}$ | $1,05\times10^{-12}$ | $3,36\times10^{-12}$ | $8,71\times10^{-20}$ |
| **UCS** [MPa] | 125 | 11,04 | 5,97 | 8,36 | 7,41 | 6,5 | 1,93 | n.m. | n.m. |
| **Vp** (dry) [km/s] | 4,95 | 1,74 | 1,38 | 1,86 | 1,19 | 2,37 | 1,34 | no signal | no signal |
| **Vp** (wet) [km/s] | 5,17 | 2,26 | 2,28 | 2,47 | 2,15 | 3,59 | 2,28 | no signal | 1,52 |

## Phreatic eruptions experiments

### Methods

The conditions for phreatic eruptions were constrained by fragmentation experiments in a shock-tube apparatus (Fig. 6a & b). Fragmentation threshold of samples and fragmentation speed was determined in a first experimental series. Subsequently the ejection speed and fragmentation efficiency of samples decompressing from 6,5 MPa and 270°C to atmospheric pressure and room temperature wash analized. (Fig. 7) The velocity of the front of the gas-particle mixture was measured via high speed videography. (Fig. 11)

Fig. 6a: Photo of the shock tube apparatus (Fragmentation bomb).

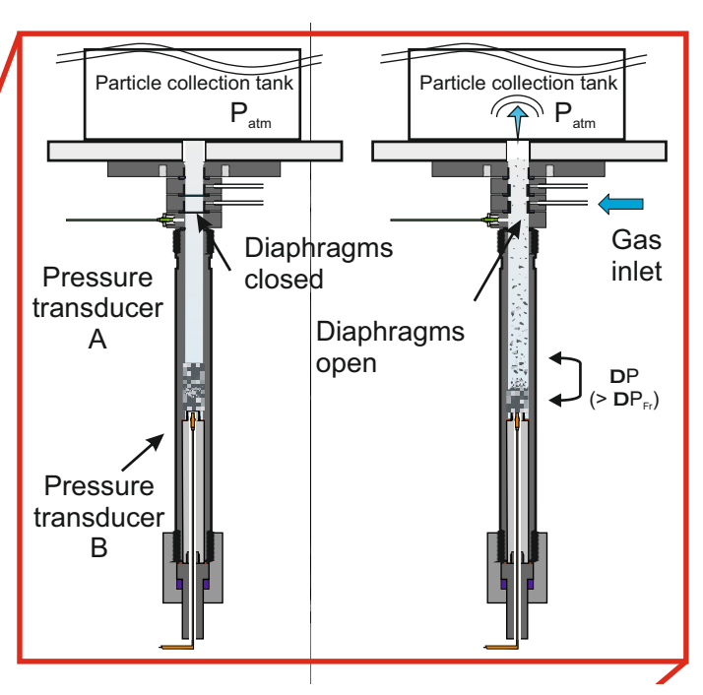

Fig. 6b: Sketch of the fragmentation apparatus with closed (left) and open diaphragms (right). The sample (l= 6 cm, d= 2.5 cm) is mounted in the high pressure autoclave. Due to a set of diaphragms, reproducible pressurization of the sample is possible. Two pressure transducers record the pressure drop during fragmentation. Modified after Scheu et al. (2006).

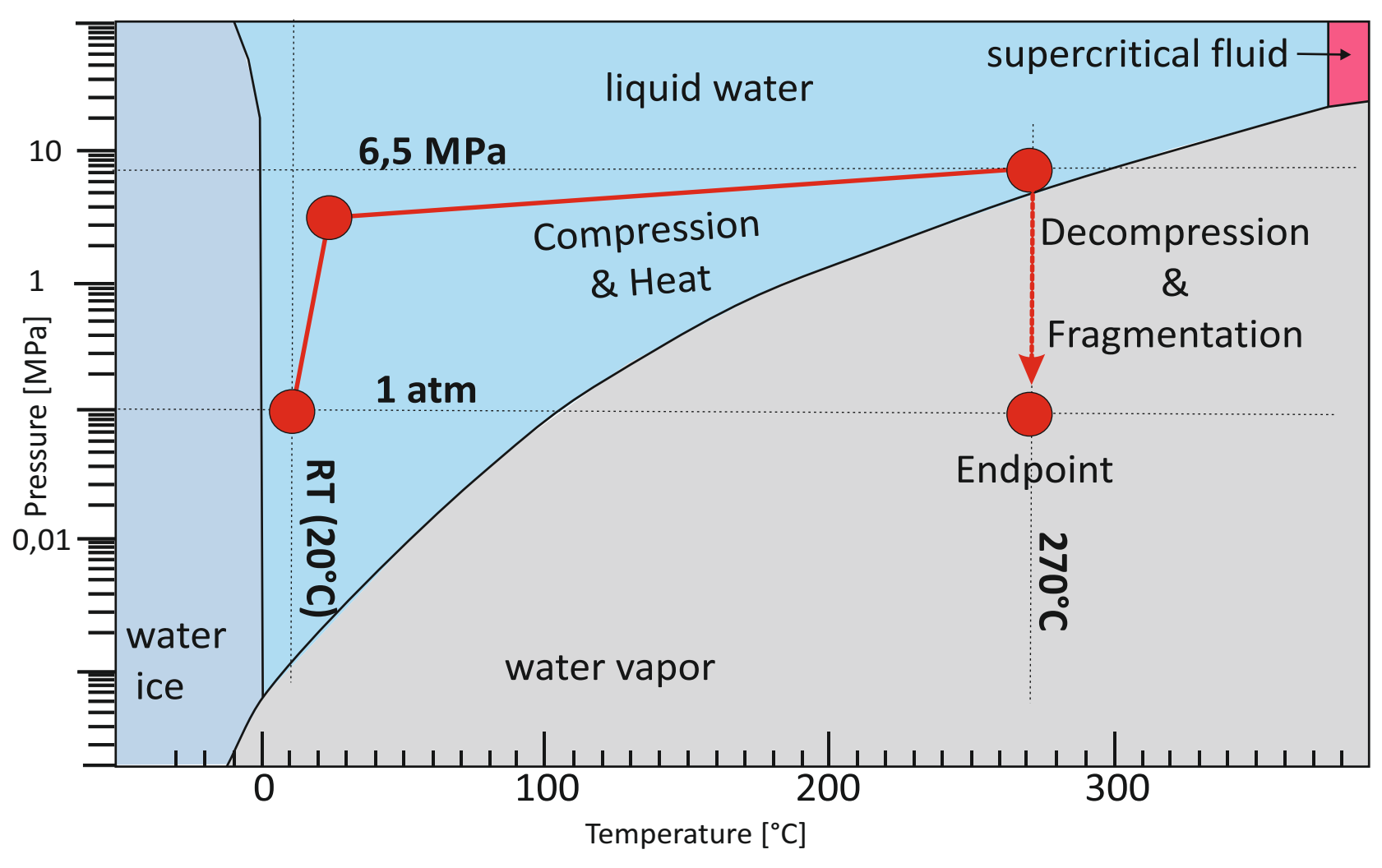

Fig. 7: Experimental conditions for phreatic eruption experiments in this study.

After pressurizing and heating the sample to a final pressure-temperature condition of 6,5 MPa and 270 °C, decompression and consequently fragmentation of the sample is triggered by controlled failure of the diaphragms, producing a rarefaction wave that travels trough the sample. During decompression the phase transition from liquid water to water vapor in the system is crossed. If the resulting pressure differential is sufficient, the sample fragments brittle in a layer-by-layer fashionh (Aldibirov and Dingwell, 2000; Fowler et al., 2010) and the particles are ejected into the voluminous tank.

### Fragmentation threshold

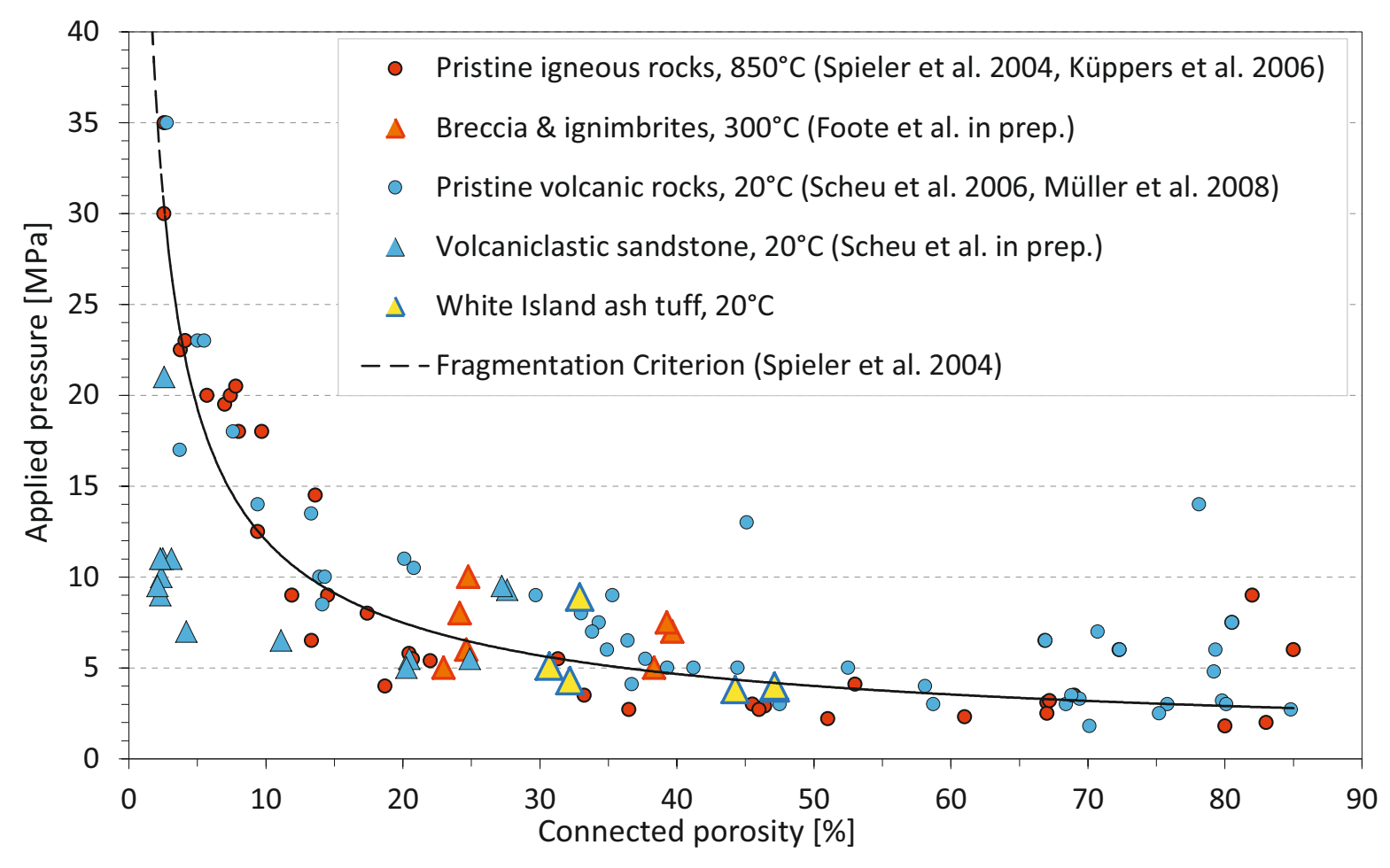

Fig. 8: Fragmentation threshold of different rocks at varying temperatures during rapid decompression. The line corresponds to the fragmentation criterion proposed by Spieler et al. 2004).

### Results

- Samples with higher porosity fragment at lower initial pore pressure – following the trend observed for pristine volcanic rocks (Fig. 8).
- Higher initial pressure as well as water saturation of samples generally leads to an increased production of fines and thus a higher fragmentation efficiency than for dry samples.
- The ejection velocity of particles increases with applied pressure and porosity as well as water saturation of samples (Fig. 9).
- Hydrothermal alteration at White Island leads to a weakening of the rocks, which may favor phreatic eruptions.

### Ejection behavior

The maximum speed and temporal decrease of partical velocities after fragmentation is controlled by the energy of the compressed gas stored in the sample. Therefore applied pressure, porosity and water content of the sample, as well as the temperature before fragmentation are crucial factors.

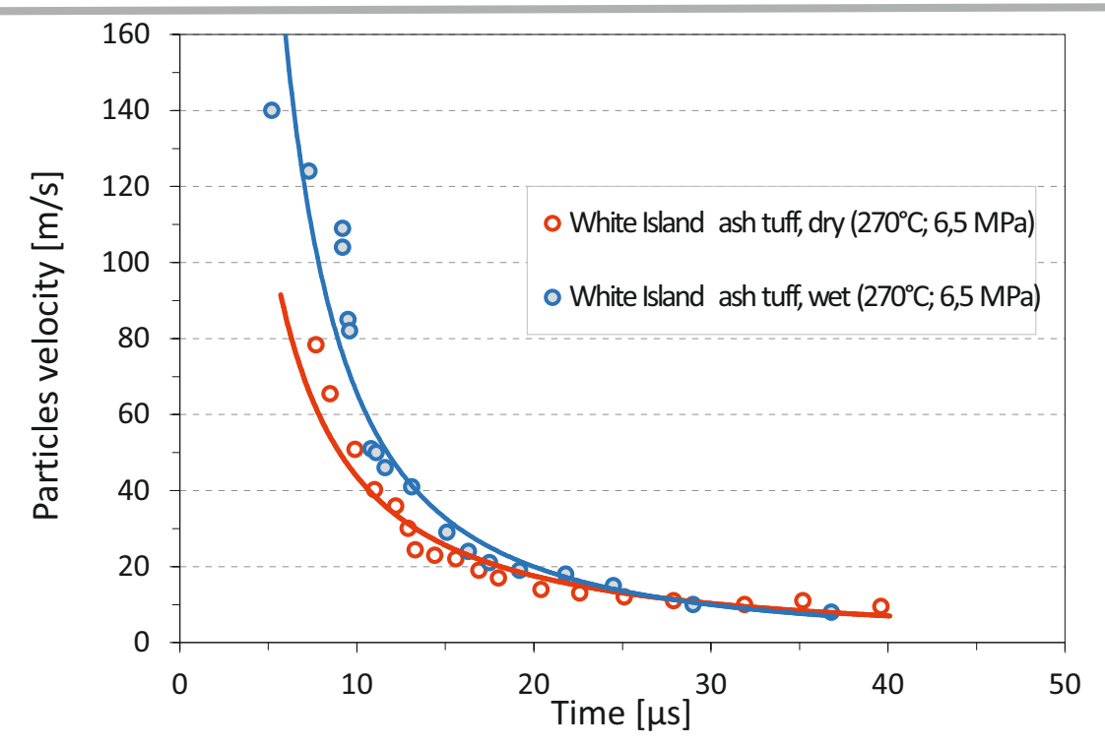

Fig. 10. Observed ejection velocities of particles during decompression experiment performed at 270°C and an initial pressure of 6,5 MPa. Particle speed was measured through image analysis of high-speed camera footage.

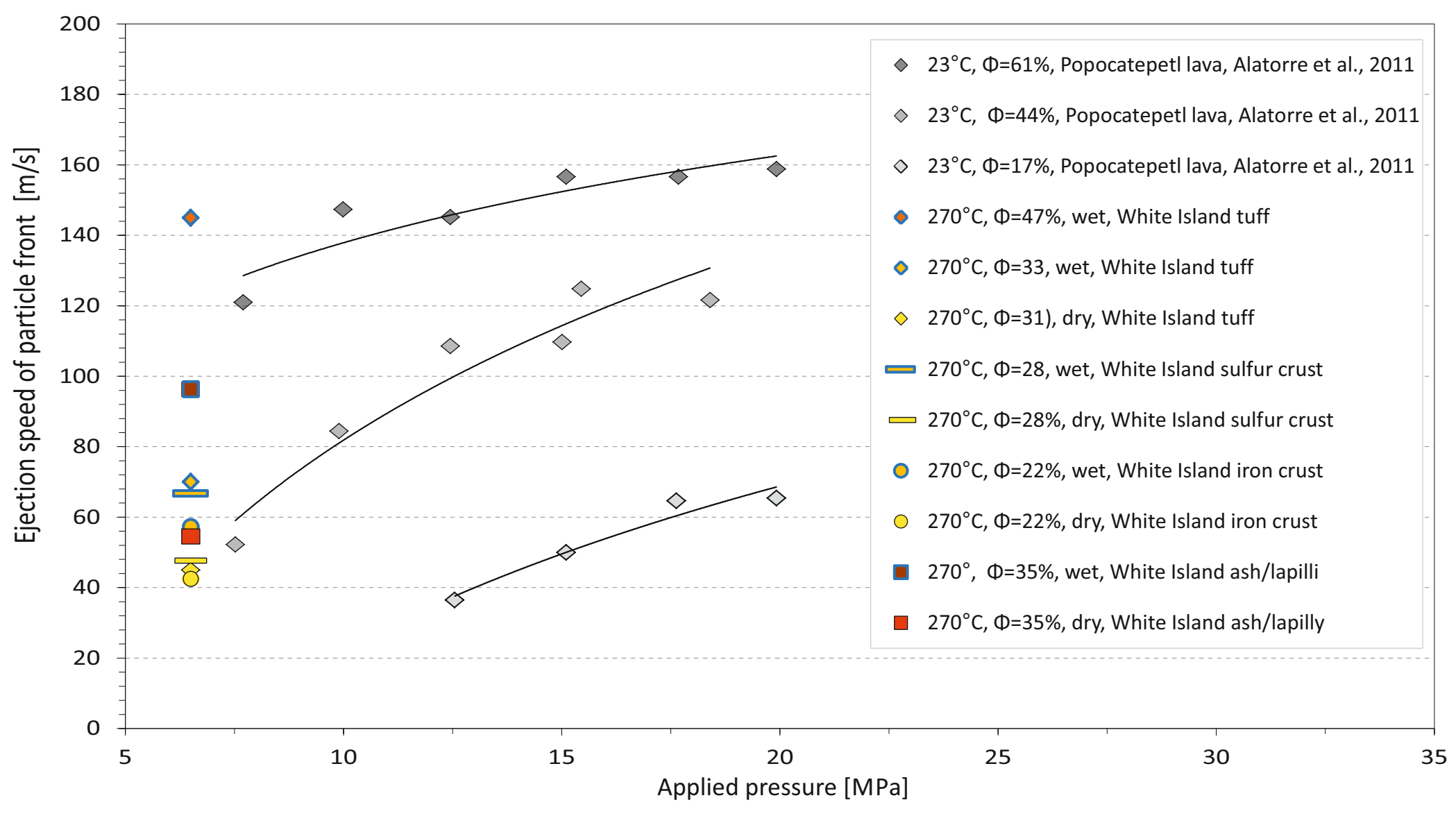

Fig. 9: Ejection speed of White Island samples compiled with Popocatepetl lava.

Fig. 11: Sequences of still-frames from movies taken by a high speed camera showing the gas particle mixture after fragmentation at 6,5 MPa and 270°C.
The sequences start with the outflow of argon gas (upper diaphragm chamber), followed by (a) argon from the autoclave and by water vapor in sequence (b) & (c) due to sample saturation. Finally a mixture of gas and particles is ejected in all sequences.
Sequence (d) shows the ejection of relative big pieces of the iron-rich crust.
The sulfur-rich crust in sequence (e) shows a different ejection behavior due to it's high sulfur content. At experimental conditions, the pure sulfur is molten, leading to a partially liquid sample and the ejection of „sulfur hairs and tears“
Ejection of unconsolidated ash/lapilli (f) characterised by an inhomogenous particle size distribution.

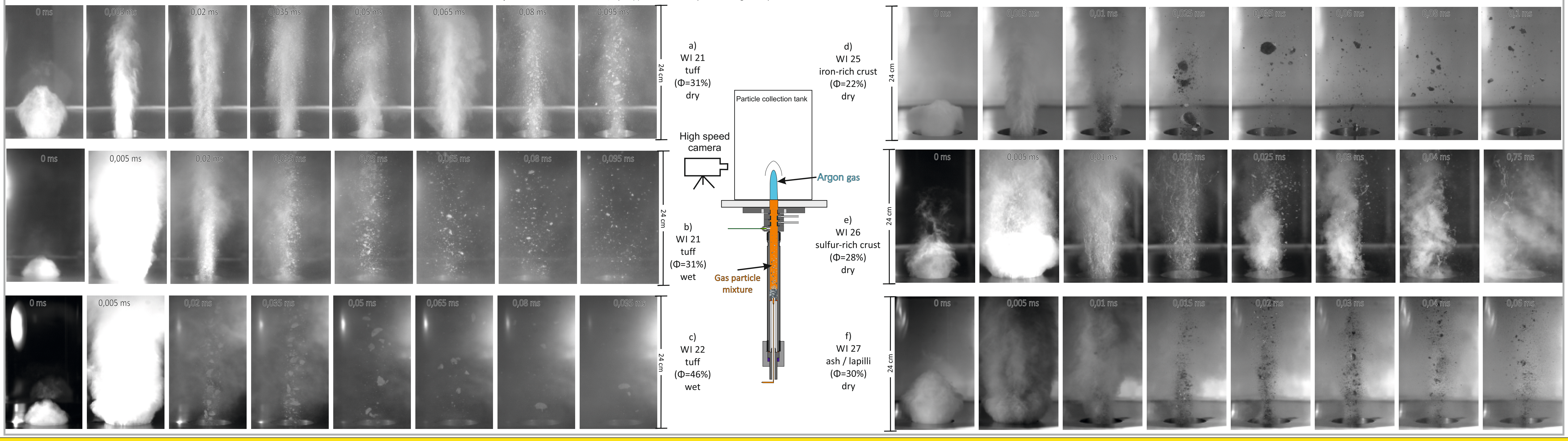

## Implications for White Island - collapse /eruption scenarios

### Stable Scenario: Magma at depth - groundwater lens

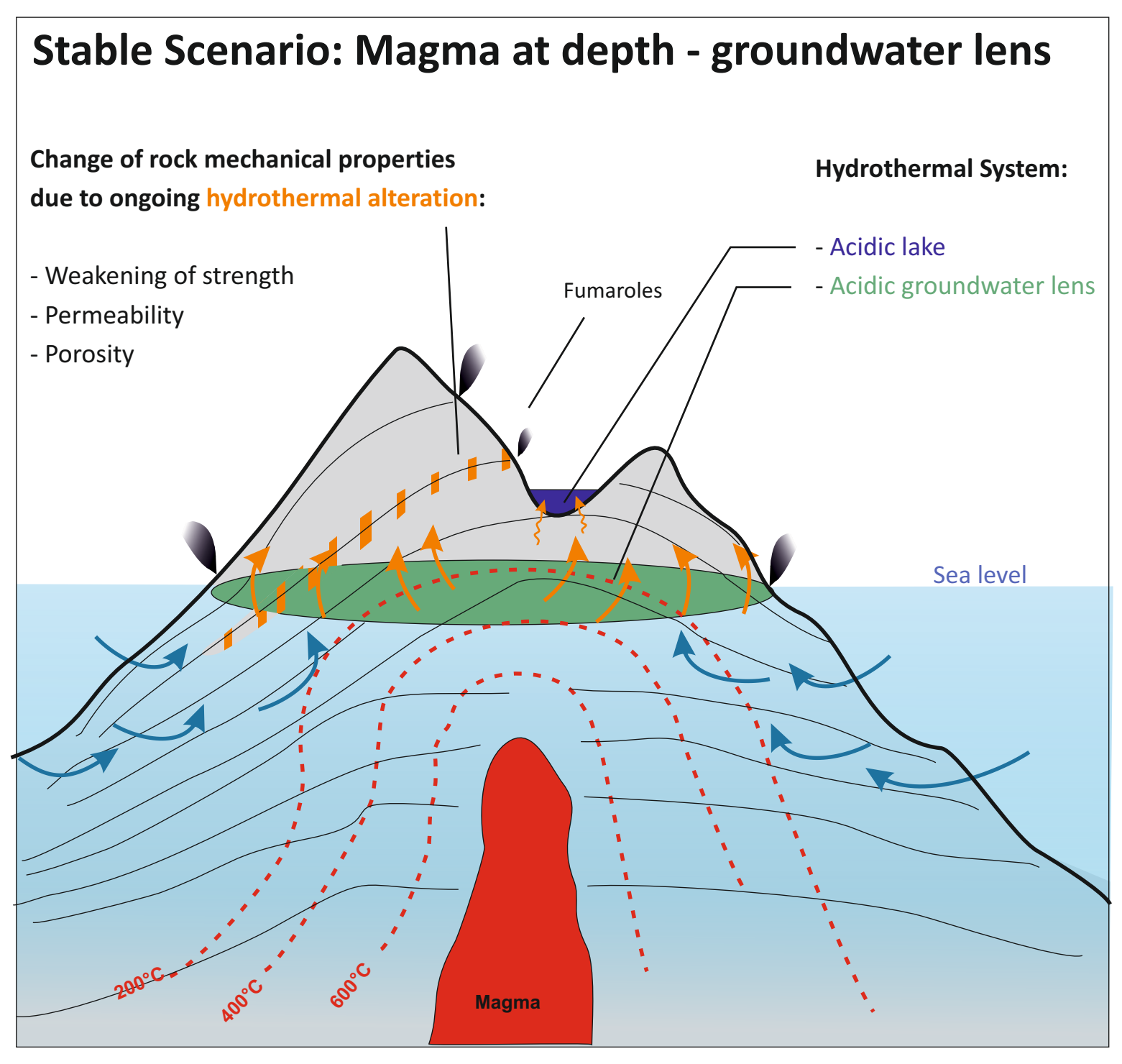

### Unstable Scenario I: Phreatic eruption causing slope destabilisation

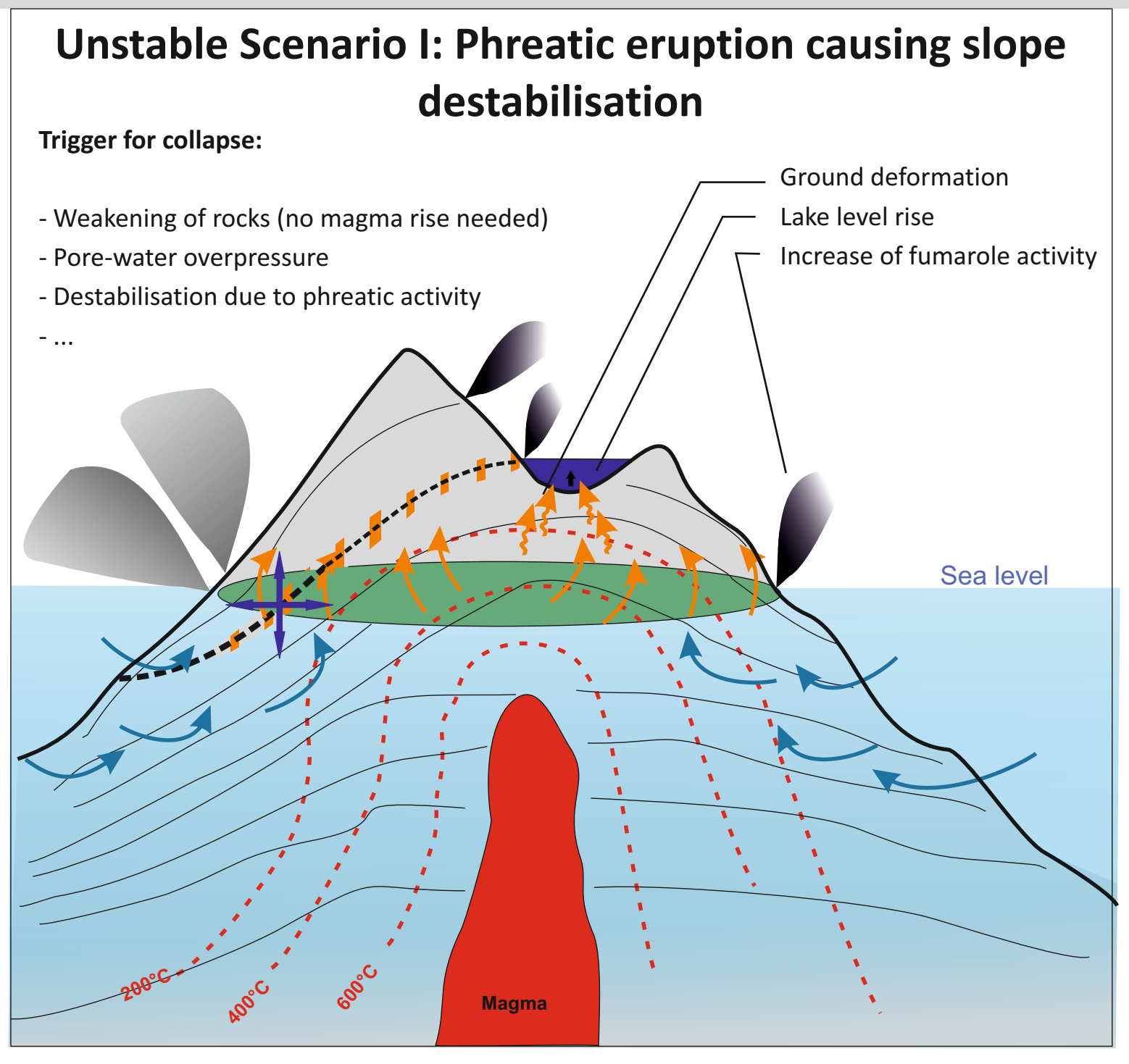

### Unstable Scenario II: Sector / lateral collapse with or without phreatic eruption

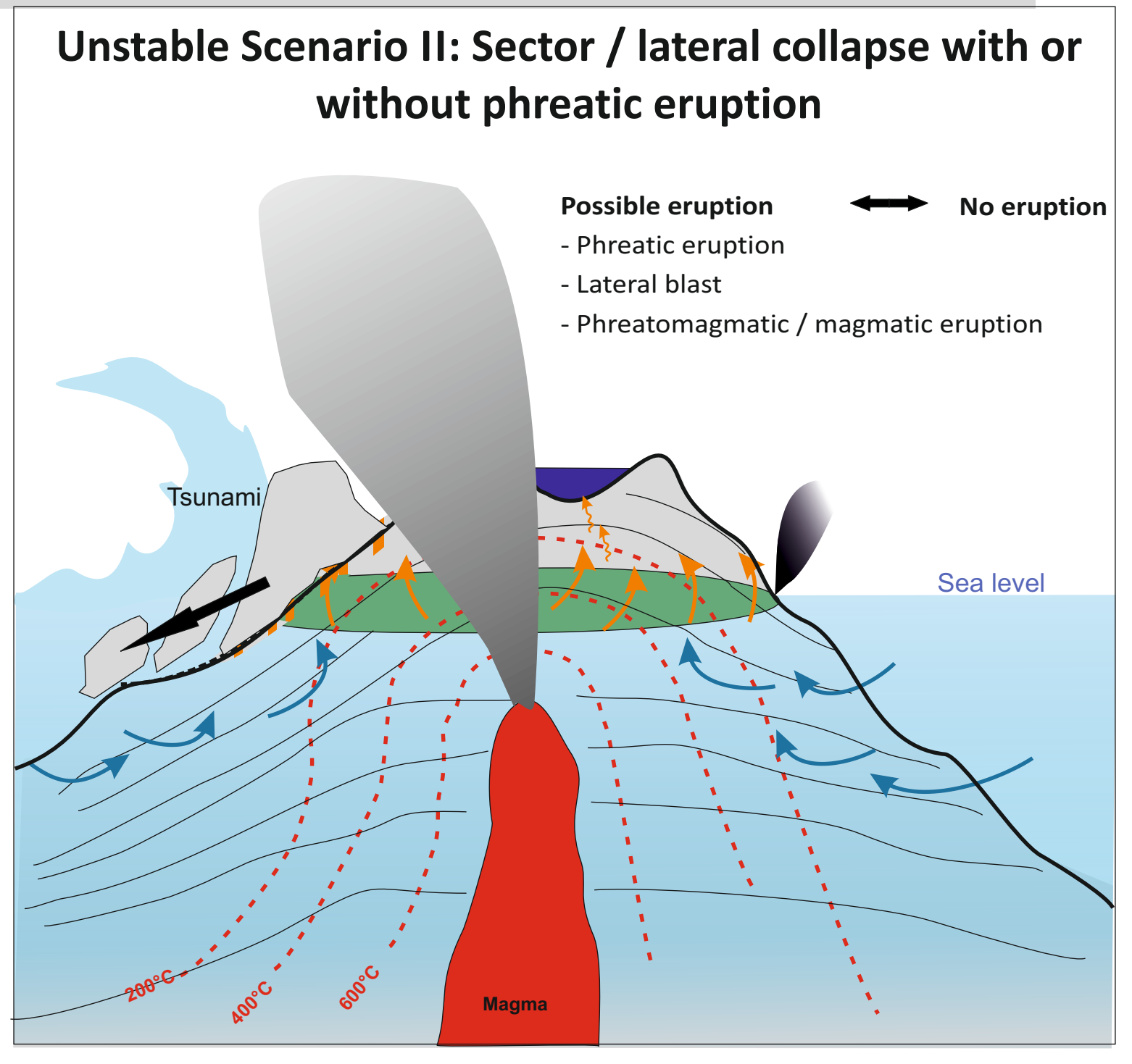

### Unstable Scenario III: Crater eruption